RSC Advances

REVIEW

View Article Online
View Journal | View Issue

Cite this: *RSC Adv.*, 2016, **6**, 45462

Relaxivity and toxicological properties of manganese oxide nanoparticles for MRI applications

Benedict You Wei Hsu,*[ab] Georgia Kirby,[cd] Aaron Tan,[ce] Alexander M. Seifalian,[f] Xu Li*[b] and John Wang[ag]

Manganese oxide nanoparticles (MONs) have received growing attention as alternative T_1 MRI contrast agents due to the association of commercial gadolinium-based contrast agents with nephrogenic systemic fibrosis. Since the seminal publication first describing the use of MONs as positive T_1 contrast agents, there is an ongoing impetus to develop MONs of higher T_1 signal intensity for better diagnostic efficacy. Indeed, various MON-based nanoprobe designs have been proposed, such as the employment of a mesoporous nanomaterial with MONs evenly dispersed within, or the traditional coating of a biocompatible layer onto the surface of MONs to form a core–shell configuration. Recent advances in this field also propose stimuli-responsive MONs that capitalize on an acidic dissolution or *in situ* reduction to release Mn^{2+} ions for a multi-fold increase in MRI contrast. However, the potential nanotoxicity of MONs remains a key obstacle to the clinical translation of MON-based T_1 contrast agents. Due to the wide variety of functionalities and physicochemical properties of MONs, there is also a lack of consensus on the toxicological properties of MONs. In addition, the r_1 relaxivity of MRI contrast agents typically decreases at higher field strength. Hence, it highlights the need to develop MON-based contrast agents with higher relaxivities. In this regard, this article aims to present a thorough review of MONs for MRI applications, with particular emphasis on their relaxivity and toxicological properties. In order to systematically review the current state-of-the-art for the development of MONs for MRI applications, the MON-based T_1 contrast agents are categorized based on the structure of the

Received 18th February 2016
Accepted 1st May 2016

DOI: 10.1039/c6ra04421b

www.rsc.org/advances

[a]*NUS Graduate School for Integrative Sciences and Engineering, National University of Singapore, Singapore. E-mail: benedict-hsu@imre.a-star.edu.sg*
[b]*Institute of Materials Research and Engineering, Agency for Science, Technology and Research (A*STAR), Singapore. E-mail: x-li@imre.a-star.edu.sg*
[c]*UCL Medical School, University College London, London, UK*
[d]*King's College, University of Cambridge, Cambridge, UK*
[e]*Biomaterials & Advanced Drug Delivery Laboratory (BioADD), Stanford University School of Medicine, Stanford University, Stanford, California, USA*
[f]*Centre for Nanotechnology & Regenerative Medicine, UCL Division of Surgery & Interventional Science, University College London, London, UK*
[g]*Department of Materials Science & Engineering, National University of Singapore, Singapore*

*Benedict You Wei Hsu pursued his PhD degree in the NUS Graduate School for Integrative Sciences & Engineering (NGS), National University of Singapore. He is currently working as a research scientist in the Institute of Materials Research and Engineering (IMRE), Agency for Science, Technology and Research (A*STAR). His research interests include the synthesis of inorganic metal oxide nanoparticles and the development of multifunctional nanomaterials for biomedical applications.*

Georgia Kirby read Medicine at King's College, University of Cambridge. She graduated with a BA in Medical Science from the University of Cambridge and is currently studying clinical medicine at University College London (UCL). Her research interests are in elucidating the physiological effects of nanoparticles in human biological systems.

nanomaterial system. Key parameters that influence the nanotoxicity of MONs are also examined while the absorption, distribution, metabolism and excretion of MON *in vivo* are evaluated to discern how long the nanoparticles will be present within the body, as well as to predict the organs or tissues in which they distribute.

1. Introduction

Apart from the non-invasive acquisition of anatomical images of high spatial resolution, magnetic resonance imaging (MRI) does not rely on the usage of radioisotopes or ionizing radiation. Hence, it has been the diagnostic tool of choice to image the central nervous system and neurological cancers.[1] However, MRI contrast arising from the variations in relaxation characteristics of different tissues of interest may not be substantial enough to generate an obvious signal contrast in the MR images. Thus, in order to improve lesion delineation and image clarification, contrast agents are often administered intravenously in patients. In the current clinical setting, gadolinium-based contrast agents (GBCAs) are commonly used. Yet, due to its recent association with nephrogenic systemic fibrosis,[2,3] there is an emerging research impetus to develop alternative T_1 MRI contrast agents that can reduce the risk of toxicity while maintaining a comparable high imaging performance to the commercial GBCAs. As such, manganese oxide nanoparticles (MONs) have received great attention in recent years, because they are potentially less toxic than its lanthanide counterparts due to the physiological function of manganese as a regulatory cofactor for many enzymes and receptors.[2] Besides, in contrast to the chelated complexes of GBCAs, the nanoparticulate characteristics of MONs can ensure a prolonged

Aaron Tan is an MBBS/PhD medical student at University College London (UCL). He obtained both his BSc in Surgical Sciences and PhD in Surgery & Bioengineering from UCL. He is currently studying clinical medicine at UCL and is a visiting scholar at the Biomaterials & Advanced Drug Delivery Laboratory (BioADD) at Stanford University. His research interests are broadly in the areas of nanoscience and nanotechnology for surgical applications.

Alexander M. Seifalian is Professor of Nanotechnology & Regenerative Medicine at University College London (UCL), and co-director of Nano-RegMed Ltd. He obtained his BSc from King's College London, and his MSc and PhD from UCL. He has received top prizes and accolades for his research in nanotechnology and artificial organs, and has published over 441 peer-reviewed papers, 41 book chapters, and holds 9 patents.

Xu Li is a Senior Scientist at Institute of Materials Research and Engineering, Agency for Science, Technology and Research. He finished his PhD study in chemistry in the Department of Chemistry, National University of Singapore (NUS) in 2001. He is an adjunct Associate Professor of the Department of Chemistry, NUS from 2012. He has published more than 80 research papers and filed 12 international patents. 5 of the patents were adopted by industry companies through technology licensing, including the one on fluorescent nanoparticles for bioimaging.

John Wang is Professor and Head of Department of Materials Science and Engineering, and Senior Faculty Member, NUS Graduate School for Integrative Sciences & Engineering (NGS), National University of Singapore. He has more than 30 years of experience in teaching and research of functional materials and materials chemistry. His current research focuses include: materials chemistry, biomaterials and nanohybrids for bioimaging and healthcare, and nanostructured materials for sustainable energy. Professor John Wang has published >300 papers in prestigious, top international refereed journals. He has been invited, on a regular basis, to give keynote/invited lectures at major international conferences/symposia/workshops.

blood circulation time,[4] thereby providing a clinically feasible scan time to achieve higher spatial MRI resolution.

Indeed, the *in vivo* applications of MONs as positive T_1 MRI contrast agents have been demonstrated in preliminary animal studies. For example, formulations of PEG–phospholipid coated MONs were successfully employed for the anatomical imaging of various brain structures in mouse.[5] Nonetheless, as MONs generally remained inferior in T_1 contrast enhancement as compared to GBCAs, there is an ongoing emphasis to develop MONs of higher T_1 relaxivity for better diagnostic efficacy. As a result, a diverse array of engineered MON-based T_1 probes have emerged. Recent advances in this field also propose nanoprobe designs which capitalize on the acidic dissolution or the *in situ* reduction of MONs to release Mn^{2+} ions for a multi-fold increase in T_1 MRI contrast.[6,7] Yet, based on the current literature, there is a paucity of reviews that particularly devote to the progress made in the last decade in the design of MONs as T_1 MRI contrast agents, as well as to assess the potential toxic effects of MONs on the human health.[3] Therefore, in this review, we aim to accomplish the following: (i) to systematically review the current state-of-the-art for the development of MONs as MRI contrast agents; (ii) to propose a systematic classification of key parameters that influences the paramagnetic relaxation enhancement and cytotoxicity assessment of MONs; and (iii) to highlight representative case studies to elucidate the *in vivo* nanotoxicological profile of MONs. This will be followed by concluding remarks and a summary of future outlook.

2. Development of MON-based nanoplatforms as MRI contrast agents

For oxides of manganese to function as strong T_1 MRI contrast agents, they must contain the divalent manganese (Mn^{2+}) ions, which are characterized by the presence of 5 unpaired electrons in their 3d shell. This creates a large magnetic moment and is responsible for inducing magnetic relaxation in the nearby nuclei.[1] Comparatively, the higher valence states of Mn tend to exhibit less effective T_1 relaxation due to fewer unpaired electrons and a smaller electron spin relaxation time.[8] As a result, the development of manganese-based T_1-weighted MRI is primarily focused on the MnO or Mn_3O_4 phase, though there are some exceptions which would be highlighted later. In addition, a nanoparticulate system which contains the magnetically active MnO component is also preferred due to the high surface concentration of Mn^{2+} ions. Hence, the nanomaterial based on MON is able to carry a large paramagnetic payload and exhibits a strong T_1 contrast enhancement even at a reduced dose. In this regard, there is a variety of MON-based nanoplatforms that have been developed for MRI as T_1 contrast agents.

2.1 Uniformly dispersed MONs in mesoporous framework

Mesoporous silica nanoparticles (MSNs) are often used as the framework with MONs evenly dispersed within. This is because they allow the dispersed MONs to be easily accessible to water molecules, which facilitates their performance as contrast agents. For example, Chen *et al.* synthesized manganese oxide–mesoporous silica nanoparticles (Mn–MSNs) using a multi-step synthetic strategy.[7,8] In their study, the MONs were first formed *in situ* inside the mesopores by the chemical reduction of $KMnO_4$ aqueous solution, followed by heat treatment in a reducing atmosphere of H_2 or Ar (Fig. 1). In a separate study, Wang *et al.* used a hydrothermal method to produce MONs-capped MSNs,[9] wherein the pre-synthesized water dispersible MONs were conjugated to the mesoporous framework *via* EDC chemistry.

Generally, these MONs-dispersed MSNs could be regarded as a new generation of stimuli-responsive MRI contrast agents because the integrated MONs would readily disintegrate in response to specific triggers to form free Mn^{2+} ions, which have a significantly higher r_1 relativity as compared to its metal oxide counterparts.[10] For example, Chen *et al.* demonstrated that the Mn–MSNs could be activated under mild acidic conditions to attain a high r_1 relaxivity of 8.81 mM^{-1} s^{-1}.[7] On the other hand, Wang *et al.* showed that exposure to a highly reducing environment could similarly cause the dissolution of MONs to release free Mn^{2+} ions for a twofold increase in T_1 signal.[9] Such stimuli-responsive behaviour can be attributed to the absence of a protective coating layer for MONs, thereby rendering the exposed nanoparticles to be particularly susceptible to degradation in mild acidic and reduction environment.[7–9] Besides MSNs, graphene oxide (GO) is another suitable candidate to construct the framework. By using a similar double redox strategy as mentioned above,[7,8] Chen *et al.* successfully dispersed MONs onto exfoliated GO nanosheets.[11] It was reported that the integrated MONs could also exhibit both pH-responsive and reduction-triggered T_1-weighted MRI, thus are highly attractive for stimuli-responsive theranostics.

Nonetheless, there is a possible weakness that can arise from the poor physico-chemical stability of MONs in the mesoporous framework. Certainly, the integrated MONs would release Mn^{2+} ions upon acidic dissolution or *in situ* reduction and this property can be utilized for stimuli-responsive dynamic T_1-weighted MRI. However, the chronic exposure to high levels of the Mn^{2+} ions can lead to an extrapyramidal disorder similar to Parkinson's disease,[12] thereby fostering concern on their clinical use. This was also indicated in studies of BxPC-3 cells incubated with MONs-dispersed MSNs wherein it was also observed that the nanoparticles exhibited no cytotoxicity until

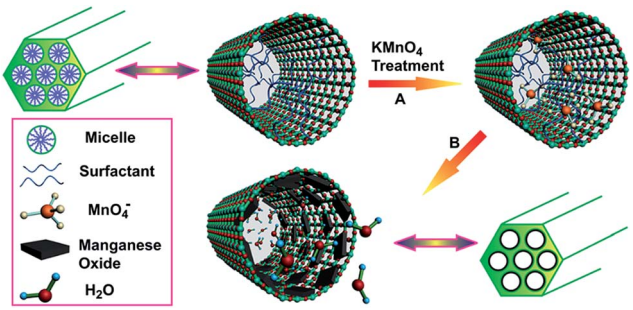

Fig. 1 Schematic illustration for the preparation of Mn–MSNs. Reprinted from ref. 8. Copyright (2012), with permission from Elsevier.

upon dissolution in a reducing environment to release free Mn^{2+} ions.[9] Nonetheless, to prevent excessive exposure to Mn^{2+} ions, a possible strategy is to confer gate-keeping properties to limit the rate of Mn^{2+} ion release. For example, light-induced switchable rotaxanes can be covalently conjugated to the surface to prepare functional MSNs that can be readily modulated by photothermal action.[13]

Another important factor of toxicity lies in the surface properties of the mesoporous framework. In this regard, unmodified MSNs, which tend to be negatively charged under physiological conditions, have been found to be more cytotoxic than their cationically modified counterparts.[14] Pasqua *et al.* showed that the thiol- or amino-functionalization of MSNs is able to reduce the toxicity of MSNs under *in vitro* conditions.[15] Similarly, Yildirim *et al.* also indicated that the hemolytic activity of MSNs could be significantly reduced by functionalization with organosilane monomers.[16] Hence, this improves the blood compatibility of MSNs, which is an important aspect to be considered for the intravenous injection of nanoparticles as MRI contrast agents. In most of the studies reported so far, synthesis of MSNs also employs structure-directing agents to generate the mesopores. Herein, the biocompatibility of the structure-directing agents is important to minimize particle-induced toxicity. On this topic, the interested reader is recommended to consult some of the excellent reviews covering the different approaches to MSN syntheses.[14]

2.2 Core–shell structured MONs

Metabolomics analyses have indicated that *in vivo* exposure to uncoated MONs could lead to disturbances to a number of metabolic processes and induce hepatic necrosis to a certain extent.[17] Hence, as indicated in Fig. 2, the MONs developed for MRI are traditionally coated by a biocompatible layer to form a core–shell configuration. For this class of nanosystem, newly-prepared MONs are typically used as a hard template for the subsequent coating of the shell material. This approach is advantageous because the synthesis of metal oxide nanoparticles with precisely controlled shape and size distribution is well-established.[18] Thus, it ensures that the resultant MONs are monodispersed and offers an avenue to tailor the magnetic properties of MONs for higher r_1 relaxivity. However, due to the inherent hydrophobicity of the resultant MONs, it also implies that the coating materials must to be able to render the MONs water-dispersible and colloidally stable in the physiological environment. In this regard, the covalent attachment of PEG chains to the coating layer is a popular strategy to improve the aqueous solubility of MONs. In particular, Gallo *et al.* reported that longer PEG molecules (~5000 Da) were preferred for nanoparticle functionalization because they prolonged the blood circulation time of MONs and afforded a greater accumulation in tumours.[19]

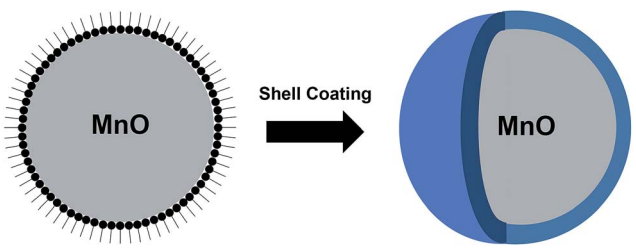

Fig. 2 Schematic representation for the biocompatible shell coating of MONs to form a core–shell configuration.

Ideally, the coating material should also be sufficiently thin so that the overall diameter remains less than 100 nm; such dimension would favour the reduced opsonisation of MONs so that the signal duration is sufficiently long for *in vivo* MR contrast enhancement. More importantly, the coating material should also allow the encapsulated manganese paramagnetic core to interact readily with the surrounding water molecules for higher r_1 relaxivity. For example, despite the excellent biocompatibility of silica, it has been argued that the r_1 relaxivity of silica-coated MONs is inevitably affected by the dense silica coating layer, which reduces the accessibility of water molecules to the MnO core.

From a toxicological standpoint, the coating material should be stable, both during storage and under *in vivo* conditions. This is because compromise of the coating layer for core–shell structured MONs can reveal the metal oxide core to release metal ions (Mn^{2+}) upon dissolution, which is toxic. This would preclude the use of numerous amphiphilic polymers as the coating material due to the inherent instability of the polymeric micelles at concentrations below the critical micelle concentration of the polymer. Nonetheless, such limitations can be overcome by crosslinking the micelle shell so that it does not readily disintegrate into its different constituents in the physiological environment. Finally, cytotoxicity of the coating material itself is a major determining factor in the overall toxicity of MONs. It has to be considered alongside with improving the r_1 relaxivity of MONs so as to develop safe nanoprobes of excellent contrast ability for practical clinical MRI applications. To this extent, we propose to categorize the core–shell structured MONs based on coating materials, which will be elaborated in a later section.

2.3 Rattle-type structured MONs

In contrast to the core–shell structured MONs, rattle-type structured MONs refers to the formation of hollow shell with a solid MON core and interstitial hollow/soft-material filled space in between. Due to the excellent loading capacity and large interior surface area of rattle-type nanostructures, they have attracted much attention in many biomedical applications such as drug storage and controlled release. To prepare rattle-type structures, most of the synthetic strategies involve the formation of core–shell nanostructures, followed by a partial removal of the shell material from inside.[20] This removal process typically entails calcination or etching in appropriate solvents. However, given that MONs are readily oxidised at high temperatures and susceptible to acidic/redox conditions, it remains a challenge to employ this strategy for the fabrication of rattle-type structured MONs. Nonetheless, Hsu *et al.* have developed an interfacial templating technique to synthesize

rattle-type structured MONs with a nanohybrid shell layer of silica and F127,[21] as illustrated in Fig. 3. In this non-conventional approach, hydrolysis and condensation of the silica precursors is confined to the interfacial region between the PPO core and the PEO corona of F127 micelles. Hence, it prevents the MON core from being in direct contact with the peripheral silica nanoshell and facilitates the passage of water molecules to the encapsulated MON since the hydroxyl groups on the MON surface are not involved in the sol–gel process.[21] Interestingly, the synthesis protocol was also facilely extended to yield hollow MONs when immersed in an acetate buffer solution, thus yielding MONs of higher surface-to-volume ratio.

In general, the rattle-type structured MONs were observed to exhibit a higher r_1 relaxivity as compared to that of other core–shell structured MONs of similar shell material. For instance, the r_1 value of silica-F127 nanohybrid encapsulated MONs was reported to be 1.17 mM^{-1} s^{-1} while the r_1 values of core–shell structured MONs were 0.08 and 0.65 mM^{-1} s^{-1}, when coated with dense silica and mesoporous silica respectively.[22] Besides the excellent imaging ability of rattle-type structured MONs, Hsu *et al.* also reported that for the formation of silica-F127 nanohybrid encapsulated MONs,[21] the silica plays an important role in reinforcing the F127 micellar structure. Thus, the colloidal stability of MONs is improved and there is minimal leaching of the Mn^{2+} ions. Moreover, a high cell viability of 83% was achieved when MDA-MB-231 cells were incubated at a high nanoparticle concentration of 224.9 μM Mn for 24 hours. This low toxicity profile is attributed to the proven biocompatibility of the two constituent materials of silica and F127 that form the shell layer.

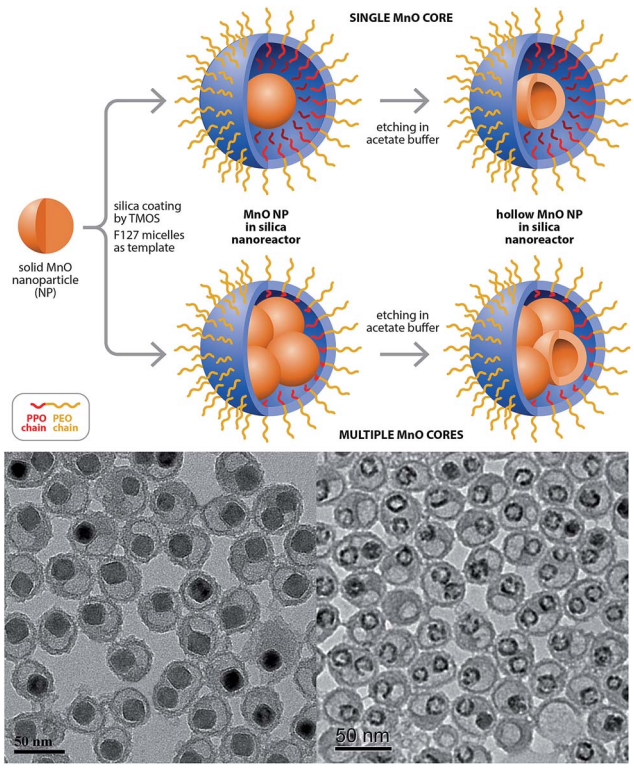

Fig. 3 Schematic representation for the preparation of rattle-typed structured MONs (solid/hollow) and their corresponding TEM images. Reproduced from ref. 21 with permission from the Royal Society of Chemistry. Reprinted with permission from ref. 38. Copyright 2015 Wiley-VCH.

2.4 Redoxable MnO_2 nanosheets

Recently, MnO_2 nanosheets have been proposed for use as T_1 MRI contrast agents. However, unlike the previous class of MON-based nanoplatforms, MnO_2 nanosheets *per se* tend to exhibit very low r_1 relaxivity. This is due to fewer unpaired electrons in the d^3 configuration of Mn^{4+} ions. As a result, the electron spin magnetic moment of Mn^{4+} ions is smaller and unable to accelerate the longitudinal relaxation of water protons effectively.[23] Instead, the MnO_2 nanosheets are uniquely designed to be intracellular glutathione (GSH)-activated MRI contrast agents.[24,25] Herein, GSH is a cytosolic biomolecule which is often present in elevated levels in cancerous tissues. As a reducing agent, GSH could also induce the dissolution of MnO_2 nanosheets and release Mn^{2+} ions for MRI contrast enhancement. It is noteworthy that these MnO_2 nanosheets could also be coupled to lanthanide-doped upconversion nanoparticles[24] or cyanine dyes[25] to incorporate fluorescence-activatable properties for cancer diagnostics applications. As shown in Fig. 4, for such hybrid probe design, the MnO_2 nanosheets would serve to quench the fluorophores effectively. However, upon cellular uptake by the targeted cancer cells, the MnO_2 nanosheets would be reduced by the intracellular GSH, thus leading to fluorescence restoration of the nanoprobe.

Nonetheless, there are concerns about the biocompatibility of MnO_2 nanosheets despite their novel stimuli-responsive MRI behaviour. Studies have suggested that the MnO_2 nanomaterial could induce significant accumulation of reactive oxygen species and result in the formation of oxidative stress in cells.[26] Hence, this would lead to DNA oxidative damage-induced necrosis and cell apoptosis. Yet, in the designs of MnO_2 nanosheets for T_1-weighted MRI,[24,25] the MONs are typically not assigned with biocompatible secondary coatings to mitigate

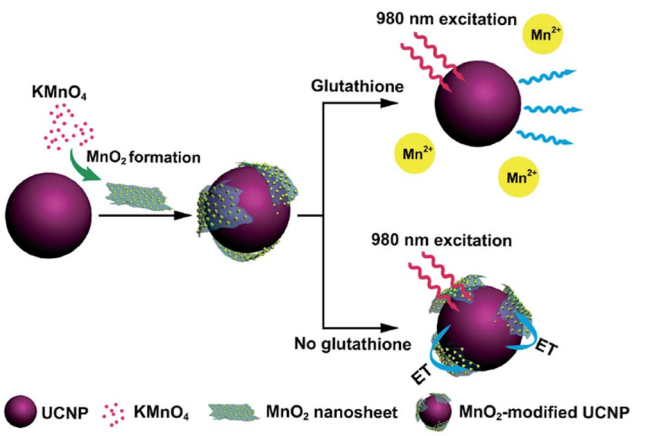

Fig. 4 Schematic illustration of MnO_2-nanosheet-modified upconversion nanoparticles for intracellular glutathione detection. Reprinted with permission from ref. 24. Copyright 2011 American Chemical Society.

their risk of nanotoxicity, which is exacerbated by a lack of toxicology-based studies for this newly-developed nanosystem. Therefore, special attention should be given to determine the absorption, distribution, metabolism and excretion (ADME) characteristics of the released free Mn^{2+} ions from the nanosheets.

2.5 MON-based heterodimer nanocomposites

The feasibility of developing MON-based hetero-nanoparticles has been demonstrated by various research groups. Touted as the next generation of Janus-type nanoparticles, it is envisioned that such nanocomposites would be highly versatile for applications in biomedical imaging due to their multi-functional capabilities. For instance, Im *et al.* have reported the synthesis of a T_1–T_2 dual modal MRI contrast agent based on Fe_3O_4/MnO hybrid nanocrystals.[27] On the other hand, Schladt *et al.* successfully constructed Au@MnO nanoflowers for concurrent magnetic and optical detection (Fig. 5).[28]

Hetero-nanoparticles are synthesized by heterogeneous nucleation of MONs onto the surface of the other inorganic counterpart (*e.g.* Fe_3O_4 or Au nanocrystals). As a result, the two inorganic domains are joined together through a small interfacial area to form an asymmetric structure with different regions of surface-active properties. Interestingly, it has been reported that a synergistic enhancement in the nanoscale properties could also be achieved in anisotropic gold and metal oxide nanoparticles (*e.g.* Au@MnO heterodimer). Unlike the isotropic analogues with a uniform wettability, these Janus-type nanoparticles would exhibit an amphiphilic character, thereby favouring their self-assembly at the oil-water interface due to the drastic decrease in interfacial tension.[29] Moreover, selective surface functionalization could also be achieved. For example, Schick *et al.* successfully encapsulated the metal oxide domain with a silica coating while leaving the gold domain untouched.[30]

In general, cell viability assays have suggested the non-cytotoxic nature of MON-based heterodimers.[28,30] However, comparison between these studies can be somewhat difficult due to the lack of uniformity in the methods used to assess toxicity and the vastly different physicochemical properties of individual compounds. Besides, the combination of multiple inorganic nanoparticles in the hetero-structure would also increase the complexity of cytotoxicity assessment since the dissolution of either inorganic core to their constituent metal ions could increase the potential toxicity risks. As has been established in core-structured MONs, the toxicity risks of these nanocomposites are also strongly influenced by the coating material used. This is because the synthesis of hetero structured MONs are typically carried out through non-hydrolytic routes, thus a suitable ligand or shell coating is required to improve their aqueous dispersibility.

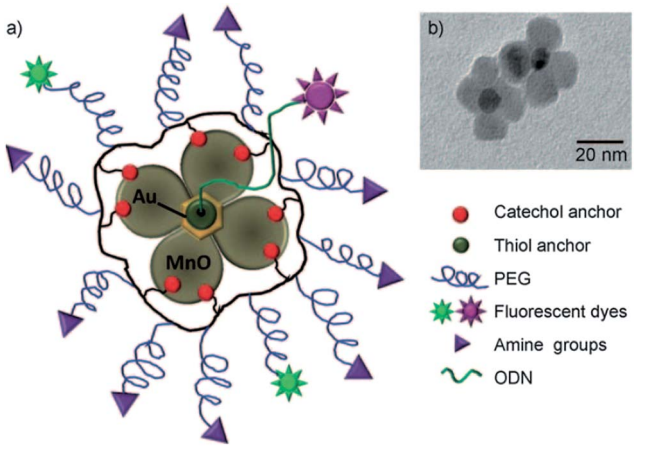

Fig. 5 (A) Schematic representation and (B) the corresponding TEM image of a polymer-coated Au@MnO nanoflower. Reprinted with permission from ref. 28. Copyright 2010 Wiley-VCH.

3. Paramagnetic relaxation enhancement

It is noteworthy that MRI is increasingly shifting to higher fields (1.5 T and above) for greater signal-to-noise ratio and higher spatial resolution and/or reduced acquisition time. Yet, the r_1 relaxivity of MRI contrast agents typically decreases at higher field strength. For example, Kim and co-workers reported that the r_1 value of mesoporous silica-coated hollow MONs decreases from 1.72 mM^{-1} s^{-1} at 1.5 T to 0.99 mM^{-1} s^{-1} at 11.7 T.[22] This can be attributed to the increased magnetization of paramagnetic MONs in higher magnetic fields, which favors the domination of T_2 effects and a reduced effectiveness of MONs to shorten the T_1 relaxation time of water.[31] Therefore, it highlights the need to develop MON-based contrast agents of higher relaxivities. Moreover, *in lieu* of the direct dose-dependent relationship on the contrast enhancement effect, a higher r_1 relaxivity is also favourable to its toxicity profile since a lower dose of the contrast agent can be administered.

Although the fundamental theories underlying the paramagnetic relaxation enhancement of T_1 contrast agents fall beyond the scope of the current review, there are several excellent sources available on this subject.[32–34] For a simplified treatment of the phenomenon, the T_1 contrast agent can be envisioned to have different solvation spheres.[31] Since the major relaxation mechanism arises from the dipole–dipole coupling between water protons and the paramagnetic ion, the inner-sphere water molecules can form stronger dipole–dipole interactions and are more susceptible to spin-lattice relaxation. Thus, in order to increase the r_1 relaxivity of MONs, current strategies are largely targeted towards increasing the availability of water molecules in closer proximity to the magnetic core. In the case of core–shell structured MONs, this can be achieved by increasing the surface-to-volume ratio of MONs, as well as structural modifications of the coating layer to enhance its water permeability.

In addition, spin-lattice relaxation is also more efficient when the tumbling rate of T_1 contrast agents (as characterized by the correlation time) corresponds closely to the proton Larmor precession frequency.[34] Yet for nanoprobe designs (*e.g.* redoxable MnO_2 nanosheets) which rely on the release of Mn^{2+} ions for T_1 MRI contrast enhancement, it is likely that the small

aqueous contrast agents have a high tumbling rate.[31] As such, the correlation time should be modulated so that it corresponds more closely to the proton Larmor precession frequency, thereby attaining a higher r_1 relaxivity.

3.1 Surface-to-volume ratio of MONs

Given that only the surface Mn^{2+} ions of the nanoparticle are mainly responsible for longitudinal water proton relaxation, a larger surface-to-volume ratio of MONs is expected to favour a more efficient rate of water exchange. For example, amongst the different nanostructured morphologies of MONs, nanoplates were observed to exhibit the highest r_1 relaxivity due to their largest surface area.[35] Na *et al.* also demonstrated that the T_1-weighted MR images of MONs were considerably brighter as the nanoparticle size decreased.[5] On the other hand, the formation of hollow MONs is another popular approach to improve the particle surface-to-volume ratio. This is typically achieved by employing a suitable etchant (*e.g.* phthalate buffer,[36] mild hydrochloric acid[22] or hydroxylamine solution[37]) to selectively remove the MnO core from a sacrificial template of MnO–Mn_3O_4 core–shell nanoparticles. Alternatively, as shown in Fig. 6, Hsu *et al.* have developed a hybrid silica nanoreactor to form well-defined hollow MONs of superior r_1 relativity of up to 2.58 mM^{-1} s^{-1} even in a high magnetic field of 7 T.[38] Herein, the hollow formation was attributed to the surface stabilization of MONs by acetate ions, followed by subsequent acidic etching of the MnO core interior. Moreover, the versatility of the silica nanoreactors to yield hollow MONs with various encapsulation morphologies was also demonstrated.

3.2 Water permeability of the coating layer

For the traditional core–shell structured MONs, the interaction of MONs with water molecules is strongly dependent on the porosity of the coating material. For instance, Peng *et al.* verified that a higher silica shell porosity would yield a larger r_1 relaxivity due to the improved accessibility of water molecules to the encapsulated MONs.[39] To generate mesopores in the silica shell, an organic structure-directing template such as cetyltrimethylammonium bromide (CTAB) is typically used.[22,39] However, it should be noted that CTAB is toxic and any incomplete removal of this surfactant can impede their use for biomedical applications. In this regard, Hsu *et al.* have proposed the design of a silica nanoshell perforated with PEO chains to act as hydrophilic nanochannels for the rapid penetration of water molecules to the MnO core.[21] Due to the highly permeable nature of the porosified silica nanoshell, the as-encapsulated MONs were shown to exhibit excellent T_1 contrast enhancement even upon cellular uptake by MDA-MB-231 cells. Hydrophilicity of the polymer ligands is an important prerequisite too, owning to a more efficient water exchange exerted by the MONs. Xing *et al.* synthesized highly water-soluble polyaspartic acid (PASP)-coated MONs which exhibited an r_1 relaxivity of 1.29 mM^{-1} s^{-1}.[40] In contrast, using the comparatively more hydrophobic poly(lactic-*co*-glycolic acid) (PLGA) as a coating material resulted in a lower r_1 relaxivity of 0.21 mM^{-1} s^{-1} of the intact MONs.[10]

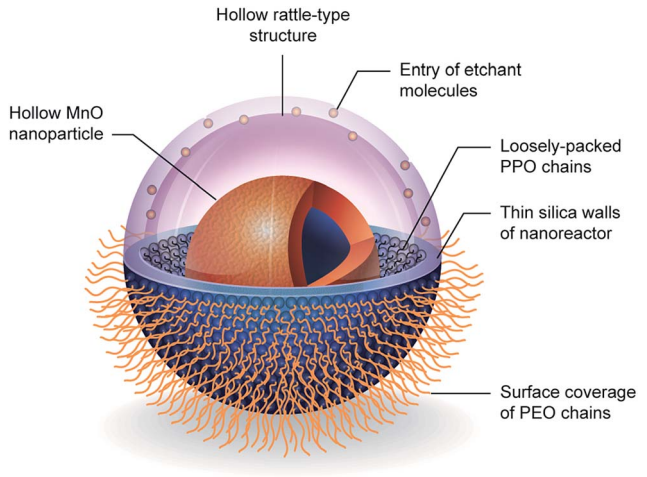

Fig. 6 3D-illustration of silica nanoreactor framework to fabricate hollow MONs. Reprinted with permission from ref. 38. Copyright 2015 Wiley-VCH.

3.3 Effect of rotational dynamics

As has been illustrated by Caravan and co-workers, the paramagnetic relaxation could be optimized by a protein binding strategy to reduce the rotational correlation time of T_1 contrast agents.[31] For instance, the r_1 value of MnL1 complex was shown to increase from 4.46 mM^{-1} s^{-1} (unbound form) to 5.78 mM^{-1} s^{-1} (protein-bound form) at 4.7 T. Similar studies have also suggested that dendrimer conjugation was another viable approach to favour a slower rotational correlation time for higher r_1 relaxivity.[41] Meanwhile, Hsu *et al.* proposed that for the encapsulation of a cluster of MONs in silica nanocarrier, the rotational diffusion of the paramagnetic payload is likely to be more restricted by the closer proximity and stronger polar interactions with the hydroxyl groups of the silica nanoshell.[38] As a result, it would be able to induce the longitudinal water proton relaxation efficiently. Indeed, the effect of rotational dynamics is a useful parameter to optimize the r_1 relaxivity, especially at low fields. Nonetheless, it is not without accompanying drawbacks. Herein, there are concerns that the binding of proteins (*e.g.* human serum albumin) could reduce the colloidal stability, thereby increasing their tendency to precipitate upon prolonged storage.[42]

4. Toxicological characteristics

Due to the wide variety of functionalities and physicochemical properties of MONs, there is a lack of consensus on the toxicological properties of MONs. It is in this context that an understanding of the toxicological characteristics of MONs is essential prior to their clinical translation. The toxicity of MONs can be induced by several mechanisms including the production of reactive oxygen species and an excessive accumulation of Mn^{2+} ions due to nanoparticle degradation. Table 1 is a summary of the *in vitro* studies performed to determine the

Table 1 Summary of toxicological studies performed to determine the potential toxicity of MONs

Type of MONs	Cell assay	Conditions	Dosage	Relaxivity	Cytotoxicity	Ref.
PEG–phospholipid	PC-3/U-87 MG/MCF7/Huh7/MRC5/NCI H460/HEK 293/HL-60 cell lines (SRB or WST-8 assays)	1×10^3 to 25×10^3 cells per well 72 h	0.045–450 μg ml^{-1}	$r_1 = 0.37$ mM^{-1} s^{-1} field: 3 T	IC_{50} range from 0.36 mM of Mn in NCI–H460 cells to 4.73 mM of Mn in MRC-5 cells	5
Manganese oxide dispersed MSNs	MCF-7 cells (MTT assay)	1×10^4 cells per well 36 h	0–400 μg ml^{-1}	$r_1 = 2.28$ mM^{-1} s^{-1} field: 3 T	Very low cytotoxic effect, IC_{50} > 400 μg ml^{-1}	8
Mn_3O_4 capped MSNs	BxPC-3 cells (MTT assay)	8×10^3 cells per well 72 h	0–0.1 μg ml^{-1}	$r_1 = 13.39$ mM^{-1} s^{-1}, $r_1 = 25.17$ mM^{-1} s^{-1} (reduced) field: 3 T	Mn_3O_4 fairly low toxicity, but released Mn^{2+} ions highly toxic	9
Poly(lactic-*co*-glycolic acid)	RG2 cells (MTS assay)	1×10^4 cells per well 48 h	50 μM [Mn^{2+}]	$r_1 = 0.21$ mM^{-1} s^{-1}, $r_1 = 7$ mM^{-1} s^{-1} (dissolved) field: 4 T	Slight toxic effect	10
PEG-1-amino undecanoic acid	M21 cells (SRB assay)	1.5×10^3 cells per well 72 h	0.005–3 mM	$r_1 = 1.44$ mM^{-1} s^{-1} field: 9.4 T	$IC_{50} = 0.14$ mM	19
Mesoporous SiO_2	Adipose-derived MSCs (MTS assay)	5×10^3 cells per well 24 h	7.6–68.6 μg ml^{-1} of Mn	$r_1 = 1.72$ mM^{-1} s^{-1} field: 1.5 T	>75% cell viability at 68.6 μg ml^{-1} of Mn	22
Polystyrene sulfonate	A549 cells (MTT assay)	4×10^3 cells per well 24 h	0–100 μg ml^{-1}	$r_1 = 2.06$ mM^{-1} s^{-1} field: 3 T	>90% cell viability	35
Mesoporous SiO_2–PEG	HeLa cells (MTT assay)	5×10^4 cells per well 24 h	5–100 μg ml^{-1}	$r_1 = 0.17$ mM^{-1} s^{-1} field: 3 T	Almost 100% cell viability at 100 μg ml^{-1}	39
DC-cholesterol and DOPE	HEK293/LLC1/A549 cells (Presto Blue assay)	72 h	0–14 μg ml^{-1}	$r_1 = 1.17$ mM^{-1} s^{-1} field: 7 T	No apparent toxicity up to 14 μg ml^{-1}	44
SiO_2–PEG–aptamer	HeLa/L02 cells (MTT assay)	5×10^4 cells per well 12 and 24 h	0–1000 μg ml^{-1}	$r_1 = 0.53$ mM^{-1} s^{-1} field: 0.5 T	>90% cell viability after 24 h at 1000 μg ml^{-1}	45
SiO_2–PEG	HeLa/MCF-7 cells (MTT assay)	24 h	0–100 μg ml^{-1}	$r_1 = 0.49$ mM^{-1} s^{-1} field: 0.5 T	>80% cell viability at 100 μg ml^{-1}	46
Dopamine–PEG–NH_2	Caki-1 cells (WST-8 assay)	1×10^5 cells per well 24 and 48 h	25–100 μg ml^{-1}	—	Low toxicity; >90% cell viability at 100 μg ml^{-1}	47
Dopamine–ssDNA	Caki-1 cells (MTT assay)	3×10^4 cells per well 12 h	6–100 μg ml^{-1}	—	Increase in cell viability at 50 μg ml^{-1} 15% cell death at 100 μg ml^{-1}	48
SiO_2–PEG/NH_2	Bone marrow-derived DCs and PMNs (Annexin-V/PI or Nicoletti staining)	2×10^5 cells per well 24 and 72 h	0.1–30 μg ml^{-1}	$r_1 = 0.47$ mM^{-1} s^{-1} field: 3 T	Negligible cytotoxicity up to 30 μg ml^{-1} for 72 h	49

potential nanotoxicity of MONs or lack thereof. Indeed, these *in vitro* assays can be used to screen hazardous nanomaterials and provide useful mechanistic insights about the nano-bio interactions. For example, MONs-dispersed MSNs were shown to exhibit a half-maximal inhibitory concentration (IC_{50}) of 400 μg ml^{-1} with breast cancer MCF-7 cells after 36 hours incubation.[8] Meanwhile, it was revealed that the high intracellular GSH concentration of cancer cells was sufficient to trigger the steady dissolution of Mn_3O_4 nanocrystals *via* a thiol-disulfide transformation to produce Mn^{2+} ions.[9] Nonetheless, given the variability in cell lines and a wide range of nanoparticle concentration used to evaluate the nanotoxicity of MONs, comparability of the *in vitro* studies may be open to doubt due to the lack of test procedure standardization. Often, the problem is complicated by insufficient characterization of the investigated nanomaterial.[43] Therefore, in the following section, we would discuss the key parameters that influence the cytotoxicity of MONs, which are essentially dependent on the nanocarrier material and the individual physicochemical properties of MONs.

4.1 Influence of nanocarrier composition

4.1.1 PEG–phospholipid micelles. In the seminal publication first describing the use of MONs as T_1 contrast agents for MRI (Fig. 7), Na *et al.* employed PEG–phospholipid micelles (DSPE–mPEG) to encapsulate MONs.[5] The potential toxicity of these PEG–phospholipid coated MONs was subsequently investigated with eight different cell lines. It was observed that the IC_{50} value ranged from 0.36 mM of Mn with NCI-H460 cells to 4.73 mM of Mn with MRC-5 cells. ICP-AES suggested no appreciable Mn-ion leaching from the MONs when kept for 7 days at room temperature while the *in vivo* biocompatibility was demonstrated by an absence of abnormal behavioural changes or signs of weight loss in mice that were injected with the PEG–phospholipid coated MONs. Shin *et al.* have extended the system of PEG–phospholipid micelles to encapsulate hollow MONs, which were reported to be relatively non-cytotoxic to MCF-7 cell lines after 72 hours.[36] Similarly, Howell *et al.* coated MONs with a phospholipid shell (DC-cholesterol and DOPE) surface-decorated with an outer corona of PEG polymers.[44] *In vitro* cytotoxicity was evaluated with HEK293 cells using the Presto Blue assay and the experimental results showed no apparent toxicity of the nanoparticles after 72 hours at a concentration of 14 μg ml^{-1}.

In general, these *in vitro* studies suggest that the PEG–phospholipid is useful to render MONs biologically compatible, as shown by the lack of observable cytotoxicity of MONs to the various human cell lines (normal and cancer). There was also no apparent MON-induced toxicity in mice *in vivo*. These findings could be attributed to the tight hydrophobic inner layer of the phospholipid micelles, which formed a strong protective barrier for the as-encapsulated MONs. Herein lies both the benefit and drawback: although the PEG–phospholipid coating enhances the physicochemical stability of MONs and significantly reduces the likelihood of Mn-ion leaching under oxidative conditions,[5] it also prevents direct water interaction with the encapsulated MON which is otherwise required for efficient water exchange.[40] As a result, the r_1 relaxivity of PEG–phospholipid coated MONs tend to be inherently low.

4.1.2 Silica shell. The second class of coating material involves a nanostructured silica shell (Fig. 8). While it may be difficult to alter the phospholipid structure without interfering with the micellar stability, the silica coating is advantageous in that it can be facilely modified by structural engineering techniques (*e.g.* generation of mesopores) to improve the r_1 relaxivity.[22] Yet, studies have indicated that such alterations to the physicochemical properties of nanostructured silica can dramatically impact its attendent toxicology.[50,51] Therefore, besides overcoming the inherent toxicity and poor water solubility of MONs under physiological conditions, it is also imperative for the nanostructured silica shell alone to exhibit excellent biocompatibility.

In this regard, toxicology of the silica shell is affected by a multitude of factors including the degree of condensation in silica, porosity and the type of ligand functionalization.[51] For instance, it has been determined that the presence of surface

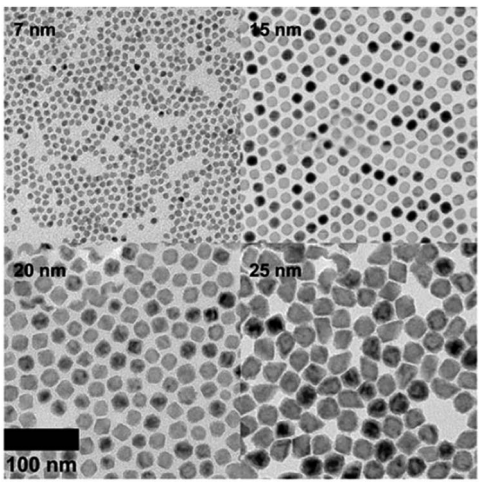

Fig. 7 TEM images of PEG–phospholipid coated MONs with different particle sizes. Reprinted with permission from ref. 5. Copyright 2007 Wiley-VCH.

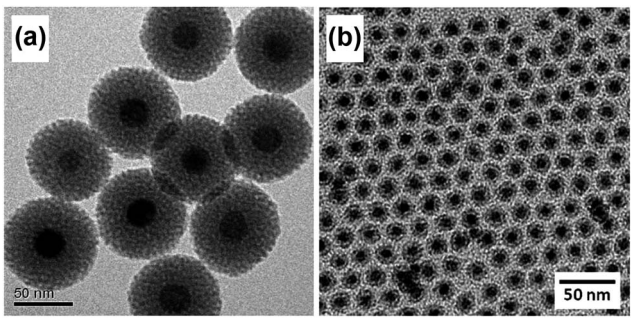

Fig. 8 TEM images of MONs coated with a uniform shell of: (a) mesoporous silica; and (b) dense silica prepared by a w/o reverse microemulsion technique. Reprinted with permission from ref. 39. Copyright 2011 American Chemical Society. Reproduced from ref. 49 with permission from the Royal Society of Chemistry.

silanol groups in amorphous silica can potentially compromise the cell membrane integrity by inducing the denaturation of membrane proteins.[52] Consequently, the potential for cell lysis is highly correlated to the degree of condensation in silica which determines the ratio of Si–OH to Si–O–Si groups on the silica surface. Lin *et al.* also investigated multifunctional nanoparticles of different silica shell nanoarchitecture; it was indicated that a non-porous silica shell would cause greater hemolytic activity than the mesoporous counterparts.[53] Interestingly, PEGylation has always been utilized for current designs of silica-coated MONs. Given that the resulting nanoparticles were generally reported to be well-tolerated in cell viability assays, it is likely that the effectiveness of PEGylation masks the toxic effects of silanol groups.

In addition, cytotoxicity studies have generally suggested that the silica shell coating is highly effective as a "capping" material to suppress the adverse effects of MONs on the cell viability. For example, Hu *et al.* encapsulated MONs within an amino-functionalized silica shell surface-conjugated with PEG chains.[45] Based on a MTT assay with HeLa and L02 cells, it was shown that the nanoparticles had minimal cytotoxicity since a high cell viability of over 90% was maintained for 24 hours even at an elevated nanoparticle concentration of 1000 μg ml^{-1}. Similar findings were reported by Yang *et al.* who synthesized PEGylated silica coated MONs with folate receptors.[46]

Besides, the silica coating also increases the resistance of MONs to degradation, thus it is effective to prevent Mn-ion leaching. In fact, Lee and co-workers reported that amongst the various coatings tested for core–shell structured MONs, the silica coating layer is most effective to reduce the likelihood of Mn-ion leaching.[54] Mice toxicity studies were also carried out by Hu *et al.*, where samples of major organs were taken at 10 days post-injection for histological examination.[45] There were no indications that the nanoparticles caused any adverse effects in the animals as no apparent cellular or tissue damage was observed in any of the organs examined. There was also no inflammatory response observed in blood smears while kidney and hepatic function indicators were at the same levels as controls, thereby affirming the non-cytotoxic nature of the silica coated MONs. It is noteworthy that the unique properties of silica-coated MONs could also render them useful for many other applications. For example, due to the catalytically active nature of the Mn_3O_4 phase, silica-coated hollow MONs have been employed for the catalysis of cyanosilylation reactions with size and shape selectivity.[37]

4.1.3 Dopamine-based ligands. Biocompatible ligands conjugated with dopamine moieties are an alternative class of coating material to functionalize MONs for applications as T_1 MRI contrast agents. This strategy has received surging interest among the scientific community because dopamine has proven to be a unique catechol anchor group that has a strong binding affinity to metal oxide nanoparticles.[55] Schladt and co-workers synthesized highly water-dispersible MONs through surface functionalization with a dopamine–PEG–protoporphyrin (DA–PEG–PP) ligand.[47] MTT assay of the DA–PEG–PP functionalized MONs confirmed a low level of cytotoxicity as a high cell viability of over 90% was observed after 48 hour incubation at a concentration of 100 μg ml^{-1}. Shukoor *et al.* also immobilized ssDNA (CpG ODN 2006) onto MONs successfully by using a dopamine-based polymeric ligand with a reactive amine group for the coupling of ssDNA.[48] The resultant nanoparticles were relatively non-toxic with concentrations up to 50 μg ml^{-1}.

Indeed, dopamine has been commonly conjugated to biocompatible polymers or proteins so as to immobilize these functional molecules onto MONs.[42,47,48] However, it has also been reported the catechol unit in dopamine tends to oxidize under aerobic conditions to form dark insoluble polymers,[55] thereby affecting the binding stability between dopamine and the metal oxide surface. Consequently, the dopamine-based ligand coating may be labile and degrading in water and biological fluids, thereby exposing the MON core complex to dissolution. This was verified by Schladt *et al.*, who showed the susceptibility of DA-PEG coated MONs to Mn-ion leaching since TEM images of the MONs had appeared rougher and less homogeneous after the leaching experiments.[49]

4.1.4 Polymer ligands. A number of *in vitro* and *in vivo* studies have been conducted to assess the toxicity of MONs stabilized by polymeric ligands. Gallo *et al.* displaced the oleic acid surface ligands of MONs with 1-aminoundecanoic acid, followed by PEG coupling for better biocompatibility.[19] *In vitro* toxicity assays indicated an IC_{50} value of 0.14 mM of Mn for the nanoparticles, which is higher than the level required for imaging *in vivo*. On the other hand, Huang *et al.* employed polystyrene sulfonate polymer to replace the hydrophobic surfactants of the MONs.[35] MTT assay revealed that the cell viability remained high (>90%) even at a high Mn concentration of 1.3 mM for 1 day. The negatively charged polymeric coating was also effective in preventing Mn-ion leaching, as ICP-AES analysis indicates that only a very small amount of free Mn^{2+} ions (~1.3%) was produced upon incubation in PBS solution at 37 °C for 48 hours. From these studies, it can be seen that engineered MONs with polymeric ligand can have vastly different outing coating bioactivity, depending on the type of polymers used. Hence, each type of MONs in this classification should be characterized individually for their potential toxicity and ADME properties. Nonetheless, based on the Pearson acid base (HSAB) concept, oxygen containing polymers would be particularly favoured because they could exhibit a high binding affinity to MONs.[55] As a result, a compact coating layer is achieved for more effective water–manganese interactions.

4.2 Influence of MON core morphology

The effect on r_1 relaxivity by changing the particle size and shape of MONs has been well-established. However, the interplay between MON morphology and toxicity is less commonly discussed. Firstly, given that smaller nanoparticles have a larger surface-to-volume ratio and higher surface reactivity, it is likely that smaller sized MONs are potentially more cytotoxic due to their greater susceptibility to Mn-ion leaching. Moreover, they would be more prone to aggregation, especially in the presence of serum proteins in the cell culture medium. Such instability in the cell medium would affect the cellular uptake of MONs during *in vitro* assays and alter the toxicological profile of MONs

accordingly. Secondly, based on studies on other inorganic nanoparticles, the toxicity of MONs is also affected by their shape and morphology. For example, it was observed that the transferrin-coated rod-shaped gold nanoparticles were less readily internalized by HeLa cells as compared to their spherical counterparts.[56] As a result, conclusions about the toxic potential of the nanoparticles would be misleading since the high cell viability arose from a decreased cellular uptake of nanoparticles instead of an improved biocompatibility of the nanoparticles. On the other hand, it has been shown that for TiO_2 nanoparticles with high aspect ratios, they may cause shape-induced toxicity by lysosomal disruption.[57] Certainly, the nano-bio interactions of MONs with varying shapes may be different, nonetheless it highlights the importance of elucidating the potential impact of particle shape on the cytotoxicity assessment of MONs.

5. Pharmacokinetics of MONs

Examining the cytotoxicity of MONs alone is inadequate for the risk assessment of MONs as T_1 MRI contrast agents for clinical use. It is also of paramount importance to understand the ADME characteristics of MONs in the living system. This will enable us to discern how long the nanoparticles will be present within the body, as well as to predict the organs or tissues in which they distribute. In this regard, the following section seeks to consider several key parameters to assess the *in vivo* nanotoxicological profile of MONs.

5.1 Opsonisation and blood circulation time

While there has been one instance of the intranasal administration of MONs in the form of nasal drops,[44] most *in vivo* studies involve an intravenous injection of MONs. Hence, the absorption is fairly straightforward and bioavailability is often near 100% since the administered dose of MONs is directly introduced into the systemic circulation. However, one of the most critical issues in association with the intravenous route of administration is the possible binding of opsonins to the nanoparticles which would facilitate their capture by macrophages in the bloodstream.[55] This is a major obstacle because it reduces the blood circulation time of MONs and prevents a clinically feasible scan time for high spatial MRI resolution.

The degree of opsonisation is affected by the overall size of nanoparticles. Larger nanoparticles (>200 nm) tend to be quickly recognized and eliminated by the reticuloendothelial system (RES). In this regard, one significant challenge for using MSNs as a platform to disperse MONs lies in the large size of the mesoporous framework, which typically ranges in the order of several hundreds of nm.[14] Chen *et al.* investigated the biodistribution of Mn–MSNs injected into mice,[8] which was observed to rapidly accumulate in the liver and spleen; such enhanced uptake suggests that the nanoparticles were highly susceptible to splenic filtration and be removed from circulation in the blood. Comparatively, the hydrodynamic size of core–shell structured MONs is usually smaller to avoid fast RES uptake, yet large enough to be above the renal clearance threshold of 5.5 nm. Hence, they are more suited for long circulation nanoparticle formulation and can be used to achieve site-specific accumulation in designated areas such as tumors. For example, Hu *et al.* have demonstrated the ability of silica coated MONs to function as tumour-specific MRI contrast agents by determining their biodistribution in tumour-bearing mice.[45] Majority of the nanoparticles were seen to accumulate in the tumour, with smaller amount taken up in the liver and spleen.

The likelihood of opsonisation is also strongly correlated to the length of PEG molecules conjugated to MONs. Gallo *et al.* investigated the bioaccumulation of PEGylated MONs in the liver, spleen and gall bladder by analysing the Mn content of the various tissues harvested from mice.[19] It was revealed that nanoparticles which were functionalised with longer PEG chains (5000 Da) exhibited a greater degree of accumulation at longer time duration than that of their shorter PEG counterparts (600 Da). This indicates that having a longer PEG length is effective to prevent adsorption of serum proteins, hence prolonging the blood circulation of MONs before their eventual uptake into the liver and spleen.

5.2 Biodistribution and clearance

Several *in vivo* studies have suggested that the biodistribution of core–shell structured MONs are fairly similar despite the variation in coating material used. Howell *et al.* showed that the highest accumulation of PEG–phospholipid coated MONs was detected in the liver after 24 hours post-injection.[44] Yang *et al.*, who traced the fate of silica coated MONs in mice 4 hours post-injection, also reported similar observations.[46] Such findings could be attributed to the coating material thickness, which necessarily increased the hydrodynamic diameter. Dense PEGylation might increase blood half-life, but it also increases the hydrodynamic diameter beyond the renal filtration threshold and precludes renal excretion from the body. Therefore, despite the systemic circulation of the nanoparticles to all bodily organs, the liver is observed to be the target organ of higher nanoparticle accumulation. Nonetheless, discrepancies in the literature exist. Chevallier *et al.* reported the presence of low Mn content in the liver and spleen by neutron activation analysis.[58] Instead, the PEGylated MONs were found to accumulate primarily in the faeces, intestine, gall bladder, kidneys and stomach, in decreasing order of magnitude. This suggests that the uptake of nanoparticles by the mononuclear phagocyte system is relatively negligible. Such atypical biodistribution data was attributed to the ultra small dimensions of MONs (6–8 nm diameter), which were also grafted with highly hydrophilic PEGylated bis-phosphonate dendrons (PDn) for the smallest possible hydrodynamic diameter. Moreover, it was indicated that over 70% of the injected dose was eliminated from the body within 48 hours as PDn grafting could be applied advantageously to confer fast renal clearance of the MONs.

As has been identified in several *in vivo* studies, the liver is likely the main organ for the clearance of nanoparticles from the blood circulation. For example, the concentration of silica coated MONs in the liver of mice was observed to peak at 12

hour post-injection before decreasing considerably by the 24 hour time point.[45] Howell *et al.* also reported that the highest accumulation of PEG–phospholipid coated MONs was detected in the liver after 24 hours, before declining significantly to the control levels by the 96 hour time point.[44] To account for a possible route of excretion in the liver, a distinction should first be made between the two major cell types of the liver: the Kupffer cells and the hepatocytes. Due to the particulate nature of MONs, they are likely to be engulfed by the Kupffer cells of the liver, which forms part of the mononuclear phagocyte system. This is usually undesirable as the phagocytized material is expected to remain in the body for a long period of time and increases the likelihood of toxicity. However, once in the Kupffer cells, the nanoparticles would be shuttled to the low pH compartments (acidic endosomes) within the cells. This results in the dissolution of MONs to release Mn^{2+} ions, which could subsequently be taken up by the adjacent hepatocytes and be excreted through the biliary pathway. Hence, the MONs are unlikely to present problems with body burdens, as verified by the absence of MON accumulation in the liver at longer times.

5.3 Interaction with blood components

Upon entry into the body, the intravenously injected MONs would interact with the various blood components including the red blood cells and platelets. Hence, from a toxicological perspective, the MONs should not compromise the red blood cell membrane and induce the rupture of red blood cells. Otherwise, the leakage of haemoglobin could potentially lead to adverse health effects such as anaemia or hypohepatia. *In vitro* hemolysis assay indicates that the hemolysis potential of MONs was 2.85%.[59] This is less than the 5% limit criterion in ASTM E2524-08, which is the standard test method for analysis of hemolytic properties of nanoparticles. Thus, it indicates that the water-dispersible MONs exhibit good hemocompatibility. Another important consideration for the toxicity profile of MONs is the particle susceptibility to trigger the inflammatory response in the body. Herein, by measuring the secretion levels of inflammatory cytokines such as interleukin 12 (IL-12) or 6 (IL-6), Schladt *et al.* quantified that silica coated MONs were not able to activate the inflammatory bone marrow-derived dendritic cells.[49] This indicated that the injected MONs would not exert any toxic effect in cells.

6. Conclusions

The development of MONs as T_1 MRI contrast agents is a burgeoning field of research with huge prospects for medical imaging applications. To achieve higher r_1 relaxivities of MONs, current design tenets include increasing the surface-to-volume ratio of MONs and water permeability of the nanocarriers, as well as optimizing the rotational correlation time of the paramagnetic payload. Moreover, the recent and present trends in this field are to further investigate *in vivo* biocompatibility, biodistribution, targeting efficiency, toxicity, biodegradability and clearance of MONs in animal models before their translation into clinical trials. Herein, the studies reviewed here suggest several key points, in particular, that the toxicity and ADME characteristics of MONs are dependent on the structure of the nanomaterial system and the type of coating materials used. To optimize the nanotoxicity evaluation of MONs, it is also necessary to thoroughly characterize the nanomaterial properties. In addition, besides an *in vitro* assessment of the MONs for their short-term cell viability, emphasis should also be placed on *in vivo* outcomes such as the opsonisation and biodistribution of the nanoparticles upon intravenous administration.

References

1 H. B. Na, I. C. Song and T. Hyeon, *Adv. Mater.*, 2009, **21**, 2133.
2 D. Pan, S. D. Caruthers, A. Senpan, A. H. Schmieder, S. A. Wickline and G. M. Lanza, *Wiley Interdiscip. Rev.: Nanomed. Nanobiotechnol.*, 2011, **3**, 162.
3 Z. Zhen and J. Xie, *Theranostics*, 2012, **2**, 45.
4 J. Kim, Y. Piao and T. Hyeon, *Chem. Soc. Rev.*, 2009, **38**, 372.
5 H. B. Na, J. H. Lee, K. An, Y. I. Park, M. Park, I. S. Lee, D. H. Nam, S. T. Kim, S. H. Kim, S. W. Kim, K. H. Lim, K. S. Kim, S. O. Kim and T. Hyeon, *Angew. Chem., Int. Ed.*, 2007, **46**, 5397.
6 T. Kim, E. J. Cho, Y. Chae, M. Kim, A. Oh, J. Jin, E. S. Lee, H. Baik, S. Haam, J. S. Suh, Y. M. Huh and K. Lee, *Angew. Chem., Int. Ed.*, 2011, **50**, 10589.
7 Y. Chen, Q. Yin, X. Ji, S. Zhang, H. Chen, Y. Zheng, Y. Sun, H. Qu, Z. Wang, Y. Li, X. Wang, K. Zhang, L. Zhang and J. Shi, *Biomaterials*, 2012, **33**, 7126.
8 Y. Chen, H. Chen, S. Zhang, F. Chen, S. Sun, Q. He, M. Ma, X. Wang, H. Wu, L. Zhang, L. Zhang and J. Shi, *Biomaterials*, 2012, **33**, 2388.
9 A. Wang, M. Guo, N. Wang, J. Zhao, W. Qi, F. Muhammad, L. Chen, Y. Guo, N. T. Nguyen and G. Zhu, *Nanoscale*, 2014, **6**, 5270.
10 M. F. Bennewitz, T. L. Lobo, M. K. Nkansah, G. Ulas, G. W. Brudvig and E. M. Shapiro, *ACS Nano*, 2011, **5**, 3438.
11 Y. Chen, P. Xu, Z. Shu, M. Wu, L. Wang, S. Zhang, Y. Zheng, H. Chen, J. Wang, Y. Li and J. Shi, *Adv. Funct. Mater.*, 2014, **24**, 4386.
12 J. Crossgrove and W. Zheng, *NMR Biomed.*, 2004, **17**, 544.
13 H. Yan, C. Teh, S. Sreejith, L. Zhu, A. Kwok, W. Fang, X. Ma, K. T. Nguyen, V. Korzh and Y. Zhao, *Angew. Chem., Int. Ed.*, 2012, **51**, 1.
14 J. M. Rosenholm, C. Sahlgren and M. Lindén, *Nanoscale*, 2010, **2**, 1870.
15 A. J. Di Pasqua, K. K. Sharma, Y. L. Shi, B. B. Toms, W. Ouellette, J. C. Dabrowiak and T. Asefa, *J. Inorg. Biochem.*, 2008, **102**, 1416.
16 L. Yildirimer, N. T. K. Thanh, M. Loizidou and A. M. Seifalian, *Nano Today*, 2011, **6**, 585.
17 J. Li, Z. Zhao, J. Feng, J. Gao and Z. Chen, *Nanotechnology*, 2013, **24**, 455102.
18 T. D. Schladt, T. Graf and W. Tremel, *Chem. Mater.*, 2009, **21**, 3183.
19 J. Gallo, I. S. Alam, I. Lavdas, M. Wylezinska-Arridge, E. O. Aboagye and N. J. Long, *J. Mater. Chem. B*, 2014, **2**, 868.

20 Y. Zhang, B. Y. W. Hsu, C. Ren, X. Li and J. Wang, *Chem. Soc. Rev.*, 2015, **44**, 315.
21 B. Y. W. Hsu, M. Wang, Y. Zhang, V. Vijayaragavan, S. Y. Wong, A. Y. C. Chang, K. K. Bhakoo, X. Li and J. Wang, *Nanoscale*, 2014, **6**, 293.
22 T. Kim, E. Momin, J. Choi, K. Yuan, H. Zaidi, J. Kim, M. Park, N. Lee, M. T. McMahon, A. Q. Hinojosa, J. W. M. Bulte, T. Hyeon and A. A. Gilad, *J. Am. Chem. Soc.*, 2011, **133**, 2955.
23 W. Xu, K. Kattel, J. Y. Park, Y. Chang, T. J. Kim and G. H. Lee, *Phys. Chem. Chem. Phys.*, 2012, **14**, 12687.
24 R. Deng, X. Xie, M. Vendrell, Y.-T. Chang and X. Liu, *J. Am. Chem. Soc.*, 2011, **133**, 20168.
25 Z. Zhao, H. Fan, G. Zhou, H. Bai, H. Liang, R. Wang, X. Zhang and W. Tan, *J. Am. Chem. Soc.*, 2014, **136**, 11220.
26 Y. Li, X. Tian, Z. Lu, C. Yang, G. Yang, X. Zhou, H. Yao, Z. Zhu, Z. Xi and X. Yang, *J. Nanosci. Nanotechnol.*, 2010, **10**, 397.
27 G. H. Im, S. M. Kim, D.-G. Lee, W. J. Lee, J. H. Lee and I. S. Lee, *Biomaterials*, 2013, **34**, 2069.
28 T. D. Schladt, M. I. Shukoor, K. Schneider, M. N. Tahir, F. Natalio, I. Ament, J. Becker, F. D. Jochum, S. Weber, O. Köhler, P. Theato, L. M. Schreiber, C. Sönnichsen, H. C. Schröder, W. E. G. Müller and W. Tremel, *Angew. Chem., Int. Ed.*, 2010, **49**, 3976.
29 N. Glaser, D. J. Adams, A. Böker and G. Krausch, *Langmuir*, 2006, **22**, 5227.
30 I. Schick, S. Lorenz, D. Gehrig, A.-M. Schilmann, H. Bauer, M. Panthöfer, K. Fischer, D. Strand, F. Laquai and W. Tremel, *J. Am. Chem. Soc.*, 2014, **136**, 2473.
31 P. Caravan, C. T. Farrar, L. Frullano and R. Uppal, *Contrast Media Mol. Imaging*, 2009, **4**, 89.
32 E. Belorizky, P. H. Fries, L. Helm, J. Kowalewski, D. Kruk, R. R. Sharp and P.-O. Westlund, *J. Chem. Phys.*, 2008, **128**, 052315.
33 D. Kruk and J. Kowalewski, *J. Chem. Phys.*, 2009, **130**, 174104.
34 N. Bloembergen and L. O. Morgan, *J. Chem. Phys.*, 1961, **34**, 842.
35 C. C. Huang, N. H. Khu and C. S. Yeh, *Biomaterials*, 2010, **31**, 4073.
36 J. Shin, R. M. Anisur, M. K. Ko, G. H. Im, J. H. Lee and I. S. Lee, *Angew. Chem., Int. Ed.*, 2009, **48**, 321.
37 R. M. Anisur, J. Shin, H. H. Choi, K. M. Yeo, E. J. Kang and I. S. Lee, *J. Mater. Chem.*, 2010, **20**, 10615.
38 B. Y. W. Hsu, M. Ng, Y. Zhang, S. Y. Wong, K. Bhakoo, X. Li and J. Wang, *Adv. Funct. Mater.*, 2015, **25**, 5269.
39 Y. K. Peng, C. W. Lai, C. L. Liu, H. C. Chen, Y. H. Hsiao, W. L. Liu, K. C. Tang, Y. Chi, J. K. Hsiao, K. E. Lim, H. E. Liao, J. J. Shyue and P. T. Chou, *ACS Nano*, 2011, **5**, 4177.
40 R. Xing, F. Zhang, J. Xie, M. Aronova, G. Zhang, N. Guo, X. Huang, X. Sun, G. Liu, L. H. Bryant, A. Bhirde, A. Liang, Y. Hou, R. D. Leapman, S. Sun and X. Chen, *Nanoscale*, 2011, **3**, 4943.
41 Z. Cheng, D. L. J. Thorek and A. Tsourkas, *Adv. Funct. Mater.*, 2009, **19**, 3753.
42 J. Huang, J. Xie, K. Chen, L. Bu, S. Lee, Z. Cheng, X. Li and X. Chen, *Chem. Commun.*, 2010, **46**, 6684.
43 H. F. Krug, *Angew. Chem., Int. Ed.*, 2014, **53**, 12304.
44 M. Howell, J. Mallela, C. Wang, S. Ravi, S. Dixit, U. Garapati and S. Mohapatra, *J. Controlled Release*, 2013, **167**, 210.
45 H. Hu, A. Dai, J. Sun, X. Li, F. Gao, L. Wu, Y. Fang, H. Yang, L. An, H. Wu and S. Yang, *Nanoscale*, 2013, **5**, 10447.
46 X. Yang, Z. Zhou, L. Wang, C. Tang, H. Yang and S. Yang, *Mater. Res. Bull.*, 2014, **57**, 97.
47 T. D. Schladt, K. Schneider, M. I. Shukoor, F. Natalio, H. Bauer, M. N. Tahir, S. Weber, L. M. Schreiber, W. E. G. Müller and W. Tremel, *J. Mater. Chem.*, 2010, **20**, 8297.
48 M. I. Shukoor, F. Natalio, M. N. Tahir, M. Wiens, M. Tarantola, H. A. Therese, M. Barz, S. Weber, M. Terekhov, H. C. Schröder, W. E. G. Müller, A. Janshoff, P. Theato, R. Zentel, L. M. Schreiber and W. Tremel, *Adv. Funct. Mater.*, 2009, **19**, 3717.
49 T. D. Schladt, K. Koll, S. Prüfer, H. Bauer, F. Natalio, O. Dumele, R. Raidoo, S. Weber, U. Wolfum, L. M. Schreiber, M. P. Radsak, H. Schild and W. Tremel, *J. Mater. Chem.*, 2012, **22**, 9253.
50 A. Liberman, N. Mendez, W. C. Trogler and A. C. Kummel, *Surf. Sci. Rep.*, 2014, **69**, 132.
51 A. E. Garcia-Bennett, *Nanomedicine*, 2011, **6**, 867.
52 C. Fruijtier-Pölloth, *Toxicology*, 2012, **294**, 61.
53 Y.-S. Lin and C. L. Haynes, *Chem. Mater.*, 2009, **21**, 3979.
54 Y. C. Lee, D. Y. Chen, S. J. Dodd, N. Bouraoud, A. P. Koretsky and K. M. Krishnan, *Biomaterials*, 2012, **33**, 3560.
55 T. D. Schladt, K. Schneider, H. Schild and W. Tremel, *Dalton Trans.*, 2011, **40**, 6315.
56 B. D. Chithrani and W. C. Chan, *Nano Lett.*, 2007, **7**, 1542.
57 R. F. Hamilton, N. Wu, D. Porter, M. Buford, M. Wolfarth and A. Holian, *Part. Fibre Toxicol.*, 2009, **6**, 35.
58 P. Chevallier, A. Walter, A. Garofalo, I. Veksler, J. Lagueux, S. Bégin-Colin, D. Felder-Flesch and M. A. Fortin, *J. Mater. Chem. B*, 2014, **2**, 1779.
59 Y. Lu, L. Zhang, J. Li, Y.-D. Su, Y. Liu, Y.-J. Xu, L. Dong, H.-L. Gao, J. Lin, N. Man, P.-F. Wei, W.-P. Xu, S.-H. Yu and L.-P. Wen, *Adv. Funct. Mater.*, 2013, **23**, 1534.